Journal of King Saud University – Science (2012) **24**, 123–129

King Saud University
Journal of King Saud University – Science
www.ksu.edu.sa
www.sciencedirect.com

ORIGINAL ARTICLE

Simultaneous heat and mass transfer in natural convection about an isothermal vertical plate

F. Khani [a,*], Abdul Aziz [b], S. Hamedi-Nezhad [a]

[a] *Department of Mathematics, Bakhtar Institute of Higher Education, Ilam, Iran*
[b] *Department of Mechanical Engineering, School of Engineering and Applied Science, Gonzaga University, Spokane, WA 99258, USA*

Received 23 July 2010; accepted 5 September 2010
Available online 24 November 2010

KEYWORDS

Vertical plate;
Natural convection;
Simultaneous heat and mass transfer;
Homotopy analysis method;
Optimal convergence-control parameter

Abstract The homotopy analysis method has been used to derive a highly accurate analytic solution for simultaneous natural convection and mass transfer from an isothermal vertical plate. Velocity, temperature, and concentration profiles are presented for a fixed Prandtl number of 0.71 and for Schmidt numbers of 0.5, 5, and 10 and for the buoyancy ratio of 0 (pure mass transfer), 0.5 (simultaneous heat and mass transfer), and 1 (pure heat transfer). The present results corroborate well with the numerical results reported in other research literature on the problem. The auxiliary parameter in the homotopy analysis method is derived by using the averaged residual error concept which significantly reduces the computational time. The use of optimal auxiliary parameter provides a superior control on the convergence and accuracy of the analytic solution.

1. Introduction

The problem of simultaneous heat and mass transfer from an isothermal vertical flat plate is of fundamental importance to the thermal science community. The pioneering contributions to the problem were made by Gebhart and Pera (1971), Mollendorf and Gebhart (1974), Taunton et al. (1970), and Bottemanne (1972a,b). Because of simultaneous heat and mass transfer, the transport process is driven by the interaction of velocity, concentration and thermal boundary layers. The velocity, concentration, and temperature profiles depend on whether the buoyancy forces due to temperature difference and concentration difference aid (aiding flow) or oppose each other (opposing flow). Bottemanne (1972a,b) considered mass transfer due to the injection of water vapor from the plate into the surrounding fluid. He found that for the aiding flow, the heat and mass transfer processes can be treated independent of each other and the results combined to predict the case when the two processes occur simultaneously. This work was examined by Schenk et al. (1976) who noted that Bottemanne's conclusion was valid because the Prandtl number $Pr = 0.71$ and Schmidt number $Sc = 0.94$ used by him were nearly the same. The numerical

* Corresponding author. Tel./fax: +98 841 2238527.
E-mail address: farzad_khani59@yahoo.com (F. Khani).

Peer review under responsibility of King Saud University.
doi:10.1016/j.jksus.2010.09.002

Production and hosting by Elsevier

computations of Schenk et al. (1976) led to the conclusion that for $Pr = 0.7$ and $0.6 < Sc < 0.9$, the mutual interaction of heat and mass transfer processes was indeed minimal and the two processes can be treated separately and the two results added. This approach gives results that are in error by about 2%, when compared with the result from the simultaneous analysis. The numerical method used by Schenk et al. (1976) involved an iterative procedure to solve the coupled similarity equations for the stream function, temperature, and concentration.

In the present work, we revisit the problem considered by Bottemanne (1972b) and provide a highly accurate analytical solution of the problem using the homotopy analysis method (HAM). In recent years, the homotopy analysis method (HAM) (Liao, 1999, 2003, 2009; Liao and Tan, 2007), has been successfully applied to many nonlinear problems in science and engineering (Molabahrami and Khani, 2009; Khani et al., 2009a,b,c; Khani and Aziz, 2009; Darvishi and Khani, 2009; Aziz and Khani, 2009). Unlike the perturbation techniques, HAM is independent of any small physical parameters. More importantly, unlike the perturbation and non-perturbation methods, HAM provides a simple way to ensure the convergence of series solution so that one can always get accurate enough approximations even for the strongly nonlinear problems. Furthermore, HAM provides the freedom to choose the so- called auxiliary linear operator so that one can approximate a nonlinear problem more effectively by means of better base functions, as demonstrated by Liao and Tan (2007). The degree of freedom is so large that even the second-order nonlinear two-dimensional Gelfand equation can be solved by means of a 4th-order auxiliary linear operator within the framework of the HAM as shown in Liao and Tan (2007). Especially, by means of the HAM, a few new solutions of some nonlinear problems (Liao, 2005, 2006) have been achieved which otherwise were not solvable by other analytic methods.

2. Formulation of the problem

The physical model and the coordinate system are shown in Fig. 1 where heat and water vapour are transferred simultaneously from the vertical flat plate to the environment. The directions of the velocity components u and v are also indicated. The boundary layer equations for this model can be written as (Bottemanne, 1972a; Schenk et al., 1976)

$$\frac{\partial u}{\partial x}+\frac{\partial v}{\partial y}=0, \tag{1}$$

$$u\frac{\partial u}{\partial x}+v\frac{\partial u}{\partial y}=g\frac{\rho_\infty-\rho}{\rho}+v\frac{\partial^2 u}{\partial y^2}, \tag{2}$$

$$u\frac{\partial \theta}{\partial x}+v\frac{\partial \theta}{\partial y}=a\frac{\partial^2 \theta}{\partial y^2}, \tag{3}$$

$$u\frac{\partial \Omega}{\partial x}+v\frac{\partial \Omega}{\partial y}=D\frac{\partial^2 \Omega}{\partial y^2}. \tag{4}$$

where ρ is the local density, ρ_∞ is the density of the fluid outside the boundary layers, θ is the local temperature difference, a is the thermal diffusivity of the fluid, Ω is the local mass fraction difference, and D is the mass diffusivity. The proper boundary conditions are:

$$\begin{cases} x>0 & y=0 & u=v=0 & \theta=\theta_0 & \Omega=\Omega_0, \\ x>0 & y=\infty & u=0 & \theta=0 & \Omega=0, \\ x=0 & y>0 & u=0 & \theta=0 & \Omega=0. \end{cases} \tag{5}$$

The classical method of solving the system of Eqs. (1)–(5) may be found in most heat and mass transfer textbooks. The same set of equations were considered by Bottemanne (1972a,b). To start the procedure, we have to introduce an expression for the density ρ as a function of the temperature θ and the concentration Ω. This expression is taken from Bottemanne (1972b), who derived it from the assumption that the ideal gas law applies to the air vapour mixture about the vertical wall. If we also introduce the well known stream function substitutions of von Mises and thereupon the similarity transformation of Pohlhausen, we finally obtain (Bottemanne, 1972b):

$$\frac{d^3 f}{d\eta^3}-2\left(\frac{df}{d\eta}\right)^2+3f\frac{d^2 f}{d\eta^2}+\delta\upsilon+(1-\delta)\omega=0, \tag{6}$$

$$\frac{d^2 \upsilon}{d\eta^2}+3Prf\frac{d\upsilon}{d\eta}=0, \tag{7}$$

$$\frac{d^2 \omega}{d\eta^2}+3Scf\frac{d\omega}{d\eta}=0, \tag{8}$$

with boundary conditions

$$f(0)=0 \quad f'(0)=0 \quad \upsilon(0)=1 \quad \omega(0)=1, \tag{9}$$

$$f'(+\infty)=0 \quad \upsilon(+\infty)=0 \quad \omega(+\infty)=0. \tag{10}$$

In this formulation f, υ, and ω represent the reduced stream function, temperature and concentration respectively; the independent variable $\eta = cyx^{-1/4}$, where the constant c depends on the buoyancy forces. The Prandtl and Schmidt numbers have their usual definitions: $Pr = \upsilon/a$ and $Sc = \upsilon/D$. The parameter δ represents essentially the ratio of the thermal buoyancy to the total body force; so is $(1-\delta)$ the ratio of concentration buoyancy to the total effect. For aiding (upward) buoyancy forces δ is necessarily $0 < \delta < 1$. In the next section, we solve the system of non-linear ordinary differential Eqs. (6)–(10) analytically using HAM.

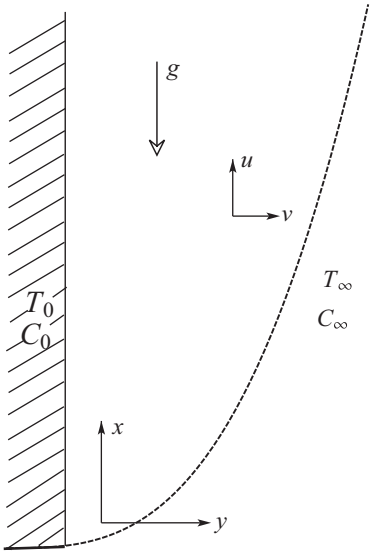

Figure 1 Physical model and coordinate system.

3. HAM solution

In view of the boundary conditions (9) and (10), $f(\eta)$, $\upsilon(\eta)$, and $\omega(\eta)$ can be expressed by the set of base functions of the form

$$\{\eta^j \exp(-n\eta) | j \geqslant 0, n \geqslant 0\} \tag{11}$$

in the form of the following series

$$f(\eta) = a_{0,0}^0 + \sum_{n=0}^{\infty}\sum_{k=0}^{\infty} a_{n,k}^k \eta^k \exp(-n\eta), \tag{12}$$

$$\upsilon(\eta) = \sum_{n=0}^{\infty}\sum_{k=0}^{\infty} b_{n,k}^k \eta^k \exp(-n\eta), \tag{13}$$

$$\omega(\eta) = \sum_{n=0}^{\infty}\sum_{k=0}^{\infty} c_{n,k}^k \eta^k \exp(-n\eta) \tag{14}$$

in which $a_{n,k}^k$, $b_{n,k}^k$, and $c_{n,k}^k$ are the coefficients. Invoking the so-called *rule of solution expressions* for $f(\eta)$, $\upsilon(\eta)$, $\omega(\eta)$ and Eqs. (9), (10) the initial guesses $f_0(\eta)$, $\upsilon_0(\eta)$, $\omega_0(\eta)$ and linear operators $\mathcal{L}_1$, $\mathcal{L}_2$, and $\mathcal{L}_3$ are

$$f_0(\eta) = (1+\eta)\exp(-\eta) - 1, \tag{15}$$

$$\upsilon_0(\eta) = \exp(-\eta), \tag{16}$$

$$\omega_0(\eta) = \exp(-\eta), \tag{17}$$

$$\mathcal{L}_1(f) = \frac{\partial^3 f}{\partial \eta^3} - \frac{\partial f}{\partial \eta}, \tag{18}$$

$$\mathcal{L}_2(\upsilon) = \frac{\partial^2 \upsilon}{\partial \eta^2} - \upsilon, \tag{19}$$

$$\mathcal{L}_3(\omega) = \frac{\partial^2 \omega}{\partial \eta^2} - \omega. \tag{20}$$

The operators $\mathcal{L}_1$, $\mathcal{L}_2$, and $\mathcal{L}_3$ have the following properties:

$$\mathcal{L}_1(c_1 + c_2\exp(-\eta) + c_3\exp(\eta)) = 0, \tag{21}$$

$$\mathcal{L}_2(c_4\exp(-\eta) + c_5\exp(\eta)) = 0, \tag{22}$$

$$\mathcal{L}_3(c_6\exp(-\eta) + c_7\exp(\eta)) = 0. \tag{23}$$

in which c_i, $i = 1, 2, \ldots, 7$ are arbitrary constants.

Let $q \in [0,1]$ denotes an embedding parameter and $\hbar_1$, $\hbar_2$, and $\hbar_3$ are non-zero auxiliary parameters. Then we construct the following *zeroth-order deformation* equations

$$(1-q)\mathcal{L}_1[\hat{f}(\eta;q) - f_0(\eta)] = q\hbar_1\mathcal{N}_1[\hat{f}(\eta;q), \hat{\upsilon}(\eta;q), \hat{\omega}(\eta;q)], \tag{24}$$

$$(1-q)\mathcal{L}_2[\hat{\upsilon}(\eta;q) - \upsilon_0(\eta)] = q\hbar_2\mathcal{N}_2[\hat{f}(\eta;q), \hat{\upsilon}(\eta;q), \hat{\omega}(\eta;q)], \tag{25}$$

$$(1-q)\mathcal{L}_3[\hat{\omega}(\eta;q) - \omega_0(\eta)] = q\hbar_3\mathcal{N}_3[\hat{f}(\eta;q), \hat{\upsilon}(\eta;q), \hat{\omega}(\eta;q)], \tag{26}$$

subject to the conditions

$$\hat{f}(0;q) = 0, \quad \hat{f}'(0;q) = 0, \quad \hat{f}'(+\infty;q) = 0, \tag{27}$$

$$\hat{\upsilon}(0;q) = 1, \quad \hat{\upsilon}(+\infty;q) = 0, \quad \hat{\omega}(0;q) = 1, \quad \hat{\omega}(+\infty;q) = 0 \tag{28}$$

where the non-linear operators are defined as:

$$\mathcal{N}_1 = \frac{\partial^3 \hat{f}(\eta;q)}{\partial \eta^3} - 2\left(\frac{\partial \hat{f}(\eta;q)}{\partial \eta}\right)^2 + 3\hat{f}(\eta;q)\frac{\partial^2 \hat{f}(\eta;q)}{\partial \eta^2} + \delta\hat{\upsilon}(\eta;q) + (1-\delta)\hat{\omega}(\eta;q),$$

$$\mathcal{N}_2 = \frac{\partial^2 \hat{\upsilon}(\eta;q)}{\partial \eta^2} + 3Pr\hat{f}(\eta;q)\frac{\partial \hat{\upsilon}(\eta;q)}{\partial \eta},$$

$$\mathcal{N}_3 = \frac{\partial^2 \hat{\omega}(\eta;q)}{\partial \eta^2} + 3Sc\hat{f}(\eta;q)\frac{\partial \hat{\omega}(\eta;q)}{\partial \eta}.$$

Clearly, when $q = 0$ the *zero-order deformation* Eqs. (24)–(26) give rise to

$$\hat{f}(\eta;0) = f_0(\eta), \quad \hat{\upsilon}(\eta;0) = \upsilon_0(\eta), \quad \hat{\omega}(\eta;0) = \omega_0(\eta).$$

When $q = 1$, they become

$$\hat{f}(\eta;1) = f(\eta), \quad \hat{\upsilon}(\eta;1) = \upsilon(\eta), \quad \hat{\omega}(\eta;1) = \omega(\eta).$$

Expanding $\hat{f}(\eta;q)$, $\hat{\upsilon}(\eta;q)$ and $\hat{\omega}(\eta;q)$ in the Maclaurin series with respect to the embedding parameter q, we obtain

$$\hat{f}(\eta;q) = f_0(\eta) + \sum_{k=1}^{\infty} f_k(\eta)q^k, \tag{29}$$

$$\hat{\upsilon}(\eta;q) = \upsilon_0(\eta) + \sum_{k=1}^{\infty} \upsilon_k(\eta)q^k, \tag{30}$$

$$\hat{\omega}(\eta;q) = \omega_0(\eta) + \sum_{k=1}^{\infty} \omega_k(\eta)q^k, \tag{31}$$

where

$$f_k(\eta) = \frac{1}{k!}\frac{\partial^k}{\partial q^k}\hat{f}(\eta;0), \quad \upsilon_k(\eta) = \frac{1}{k!}\frac{\partial^k}{\partial q^k}\hat{\upsilon}(\eta;0),$$

$$\omega_k(\eta) = \frac{1}{k!}\frac{\partial^k}{\partial q^k}\hat{\omega}(\eta;0). \tag{32}$$

Assuming that above series converges at $q = 1$, we have

$$f(\eta) = f_0(\eta) + \sum_{k=1}^{\infty} f_k(\eta), \tag{33}$$

$$\upsilon(\eta) = \upsilon_0(\eta) + \sum_{k=1}^{\infty} \upsilon_k(\eta), \tag{34}$$

$$\omega(\eta) = \omega_0(\eta) + \sum_{k=1}^{\infty} \omega_k(\eta). \tag{35}$$

Differentiating the *zero-order deformation* Eqs. (24)–(28) m times with respect to q, then setting $q = 0$, and finally dividing by $m!$, we have the *high-order deformation* equations ($m \geqslant 1$)

$$\mathcal{L}_1[f_m - \chi_m f_{m-1}] = \hbar_1\mathcal{R}_m, \tag{36}$$

$$\mathcal{L}_2[\upsilon_m - \chi_m \upsilon_{m-1}] = \hbar_2\mathcal{S}_m, \tag{37}$$

$$\mathcal{L}_3[\omega_m - \chi_m \omega_{m-1}] = \hbar_3\mathcal{K}_m, \tag{38}$$

with the boundary conditions:

$$f_m(0) = f_m'(0) = f_m'(+\infty) = 0, \tag{39}$$

$$\upsilon_m(0) = \upsilon_m(+\infty) = 0, \tag{40}$$

$$\omega_m(0) = \omega_m(+\infty) = 0, \tag{41}$$

where

$$\chi_m = \begin{cases} 0, & m = 1, \\ 1, & m > 1, \end{cases}$$

and

$$\mathcal{R}_m = f_{m-1}''' - 2\sum_{i=0}^{m-1} f_i' f_{m-1-i}' + 3\sum_{i=0}^{m-1} f_i f_{m-1-i}'' + \delta\upsilon_{m-1} + (1-\delta)\omega_{m-1},$$

$$\mathcal{S}_m = \upsilon_{m-1}'' + 3Pr\sum_{i=0}^{m-1} f_i \upsilon_{m-1-i}',$$

$$\mathcal{K}_m = \omega_{m-1}'' + 3Sc\sum_{i=0}^{m-1} f_i \omega_{m-1-i}'.$$

Then the solutions for Eqs. (36)–(38) can be expressed by

$$f_m(\eta) = \chi_m f_{m-1} + \hbar_1 \mathcal{L}_1^{-1}[\mathcal{R}_m] + d_1 + d_2 \exp(-\eta) + d_3 \exp(\eta),$$
$$\upsilon_m(\eta) = \chi_m \upsilon_{m-1} + \hbar_2 \mathcal{L}_2^{-1}[\mathcal{S}_m] + d_4 \exp(-\eta) + d_5 \exp(\eta),$$
$$\omega_m(\eta) = \chi_m \omega_{m-1} + \hbar_3 \mathcal{L}_3^{-1}[\mathcal{K}_m] + d_6 \exp(-\eta) + d_7 \exp(\eta),$$

where d_i are constants to be determined by boundary conditions (39)–(41), $\mathcal{L}_1^{-1}, \mathcal{L}_2^{-1}$ and $\mathcal{L}_3^{-1}$ denote the inverse linear operators of $\mathcal{L}_1$, $\mathcal{L}_2$, and $\mathcal{L}_3$ so that the problem is closed. For example, solving the *1st-order deformation* equation, we have

$$f_1(\eta) = \frac{35\hbar_1}{108} + e^{-\eta}\left(-\frac{\hbar_1}{27} - \hbar_1\eta^2\right) + e^{-2\eta}\left(-\frac{31\hbar_1}{108} - \frac{11\hbar_1\eta}{18} - \frac{\hbar_1\eta^2}{6}\right),$$
$$\upsilon_1(\eta) = e^{-\eta}\left(\frac{7\hbar_2 Pr}{3} - \frac{\hbar_2\eta}{2} - \frac{3\hbar_2 Pr\eta}{2}\right) + e^{-2\eta}\left(-\frac{7\hbar_2 Pr}{3} - \hbar_2 Pr\eta\right),$$
$$\omega_1(\eta) = e^{-\eta}\left(\frac{7\hbar_3 Sc}{3} - \frac{\hbar_3\eta}{2} - \frac{3\hbar_3 Sc\eta}{2}\right) + e^{-2\eta}\left(-\frac{7\hbar_3 Sc}{3} - \hbar_3 Sc\eta\right).$$

With the aid of mathematical software, such as MATHEMATICA or MAPLE, it is easy to derive the higher order solutions.

4. Results and discussion

At the mth-order approximation, we have the analytic solutions of (6)–(8), namely

$$f(\eta) \approx \sum_{k=0}^{m-1} f_k(\eta), \quad \upsilon(\eta) \approx \sum_{k=0}^{m-1} \upsilon_k(\eta), \quad \omega(\eta) \approx \sum_{k=0}^{m-1} \omega_k(\eta).$$

As pointed out by Liao (2009), the convergence and the rate of approximation for the HAM solution strongly depends upon $\hbar$. In order to obtain the admissible value of $\hbar$ for the present problem, we set $\hbar_1 = \hbar_2 = \hbar_3 = \hbar$ and the $\hbar$-curves are plotted for 13th-order of approximations. This helps us to determine the valid region of $\hbar$, which corresponds to the line segment almost parallel to the horizontal axis. Figs. 2–4 show the valid region of $\hbar$ for $f'''(0)$, $\upsilon''(0)$, and $\omega''(0)$, respectively. The parameters chosen for establishing the region of convergence were $Pr = 0.71$, $Sc = 0.1$, and $\delta = 0.5$. In fact, the interval for the admissible values of $\hbar$ shrinks as the parameters increase. In theory, at the mth-order of approximation, one can define the exact square residual errors

$$\Delta_{i,m} = \int_0^{+\infty} \left(\mathcal{N}_i\left[\sum_{j=0}^{m} f_j,\ \sum_{j=0}^{m} \upsilon_j,\ \sum_{j=0}^{m} \omega_j\right]\right)^2 d\eta, \quad i = 1,\ 2,\ 3. \tag{42}$$

Note that $\Delta_{i,m}$ contains at most three unknown convergence-control parameters $\hbar_1$, $\hbar_2$, and $\hbar_3$, even at very high order of approximation. Obviously, the more quickly $\Delta_{i,m}$ decreases to zero, the faster the corresponding homotopy-series solution converges. So, at the given order of approximation m, the corresponding optimal values of the convergence-control parameters $\hbar_1$, $\hbar_2$, and $\hbar_3$ are given by the minimum of $\Delta_{i,m}$, corresponding to a set of three nonlinear algebraic equations

$$\frac{\partial \Delta_{i,m}}{\partial \hbar_1} = 0, \quad \frac{\partial \Delta_{i,m}}{\partial \hbar_2} = 0, \quad \frac{\partial \Delta_{i,m}}{\partial \hbar_3} = 0. \tag{43}$$

Unfortunately, the exact square residual error $\Delta_{i,m}$ defined by (42) consumes too much CPU time to calculate even if the order of approximation is not very high, and thus is often useless

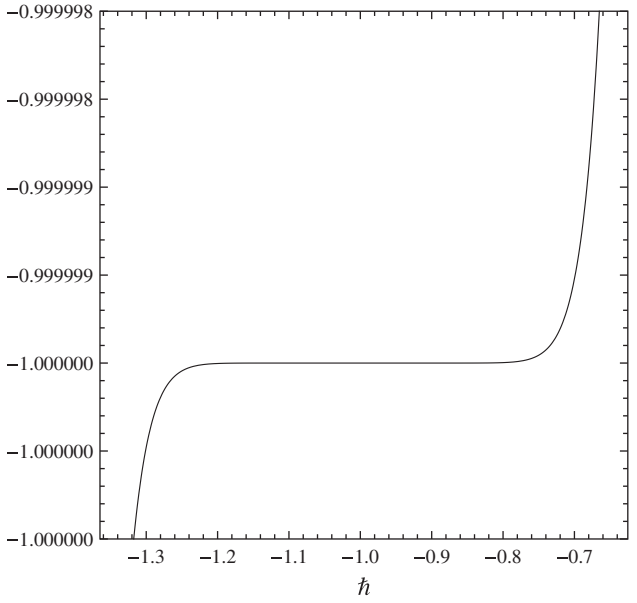

Figure 2 The curve of the $f'''(0)$ versus $\hbar$ at $Pr = 0.71$, $Sc = 0.1$, and $\delta = 0.5$ for the 13th-order approximation when $\hbar_1 = \hbar_2 = \hbar_3 = \hbar$.

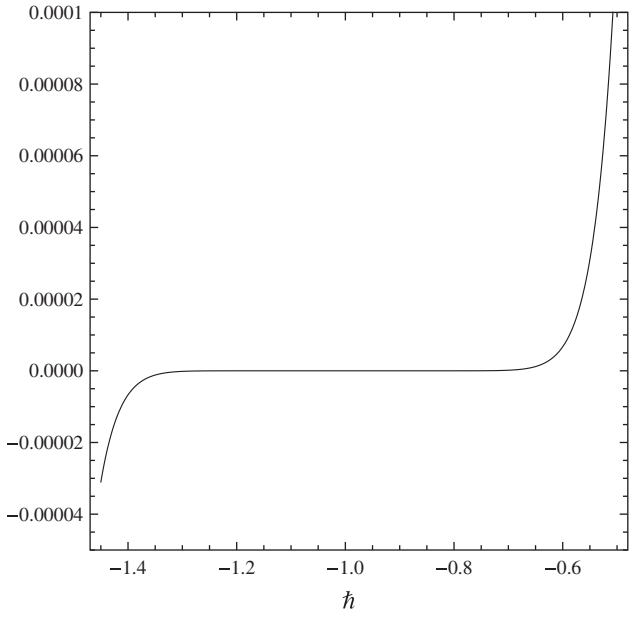

Figure 3 The curve of the $\upsilon''(0)$ versus $\hbar$ at $Pr = 0.71$, $Sc = 0.1$, and $\delta = 0.5$ for the 13th-order approximation when $\hbar_1 = \hbar_2 = \hbar_3 = \hbar$.

in practice. To overcome this disadvantage, Liao (2010) introduced a more efficient definition of the residual error to replace (42). Thus, to greatly decrease the CPU time, we use here the so-called averaged residual error defined by

$$E_{i,m} = \frac{1}{K}\sum_{s=0}^{K}\left(\mathcal{N}_i\left[\sum_{j=0}^{m} f_j(s\Delta\eta),\ \sum_{j=0}^{m} \upsilon_j(s\Delta\eta),\ \sum_{j=0}^{m} \omega_j(s\Delta\eta)\right]\right)^2, \quad i = 1,\ 2,\ 3. \tag{44}$$

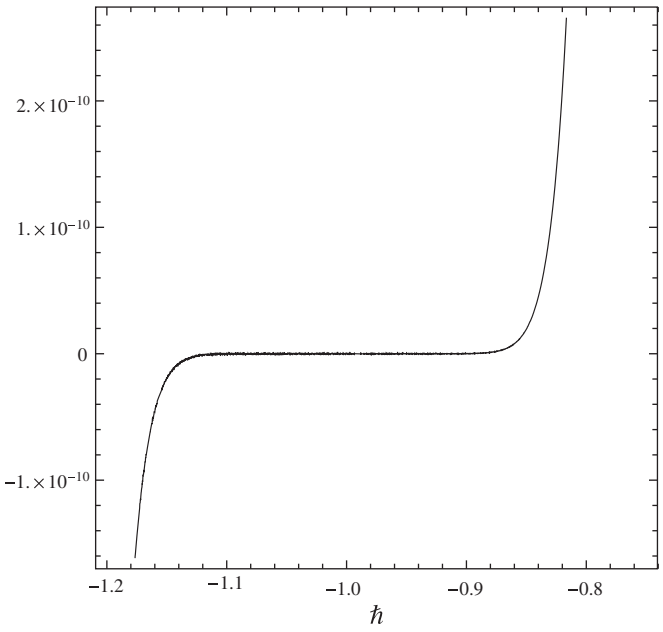

Figure 4 The curve of the $\omega''(0)$ versus $\hbar$ at $Pr = 0.71$, $Sc = 0.1$, and $\delta = 0.5$ for the 13th-order approximation when $\hbar_1 = \hbar_2 = \hbar_3 = \hbar$.

where $\Delta\eta = 10/K$ and $K = 20$ for this problem. The averaged residual error $E_{i,m}$ defined by (44) can give good enough approximation of the optimal convergence-control parameters. However, the CPU time to get the averaged residual error $E_{i,m}$ is much less than that to calculate the exact residual error $\Delta_{i,m}$ in case of $m > 6$. We reports the optimal values of $\hbar_1$, $\hbar_2$, and $\hbar_3$ for different values of Sc and δ at 13th-order approximation in Tables 1 and 2.

Fig. 5 shows the distribution of the vertical component of the velocity as a function of the similarity variable for Schmidt number $Sc = 0.5$, 5, and 10 with $Pr = 0.71$ and $\delta = 0.5$. In each case, the peak velocity occurs at $\eta = 1$. However, the magnitude of the peak velocity decreases as the Schmidt number Sc increases. This behavior is consistent with the velocity profiles presented in Fig. 1 of Schenk et al. (1976). The temperature profiles corresponding to the velocity profiles in Fig. 5

Table 1 Optimal values of $\hbar_1$, $\hbar_2$, and $\hbar_3$ for different values of Sc at 13th-order approximation.

$Pr = 0.71$ $\delta = 0.5$			
Sc	$\hbar_1$	$\hbar_2$	$\hbar_3$
0.5	−1.23	−1.21	−1.22
5	−0.95	−1.10	−1.13
10	−0.72	−0.92	−0.93

Table 2 Optimal values of $\hbar_1$, $\hbar_2$, and $\hbar_3$ for different values of δ at 13th-order approximation.

$Pr = 0.71$ $Sc = 0.1$			
δ	$\hbar_1$	$\hbar_2$	$\hbar_3$
0	−1.12	−1.02	−1.05
0.5	−0.84	−1.10	−0.87
1	−0.83	−0.81	−0.84

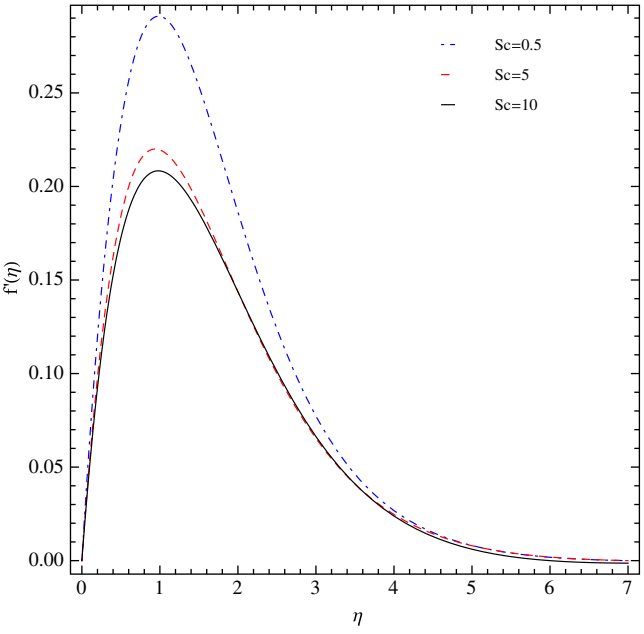

Figure 5 Influence of Sc on $f'(\eta)$ at $Pr = 0.71$ and $\delta = 0.5$ at the optimal values of $\hbar_1$, $\hbar_2$, and $\hbar_3$.

are illustrated in Fig. 6. These profiles show that as the Schmidt number Sc increases, the local temperature in the thermal boundary layer increases. The same pattern can be gleaned from the temperature distributions in Fig. 1 of Schenk et al. (1976). The concentration profiles corresponding to the velocity profiles of Fig. 5 and temperature profiles of Fig. 6 are provided in Fig. 7. Both the thickness of the concentration boundary layer and the local concentration decrease sharply as the Schmidt number increases. The thinning of the concentration boundary layer with the increase in Sc can also be observed distinctly in the results presented in Schenk et al. (1976).

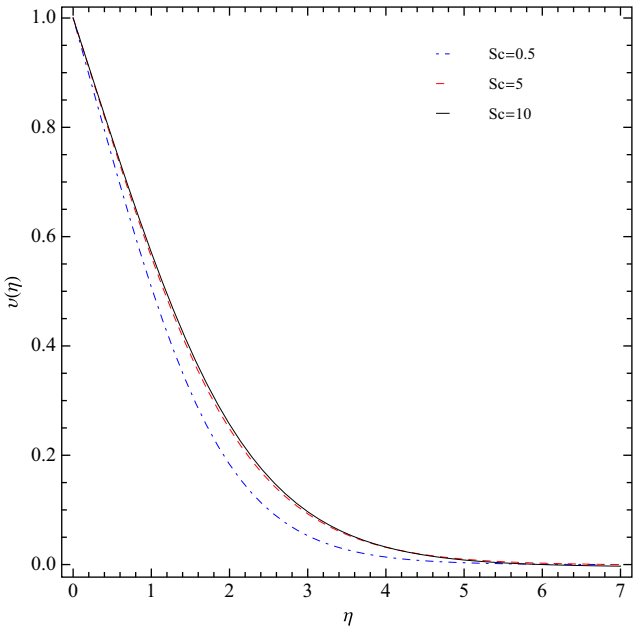

Figure 6 Influence of Sc on $\upsilon(\eta)$ at $Pr = 0.71$ and $\delta = 0.5$ at the optimal values of $\hbar_1$, $\hbar_2$, and $\hbar_3$.

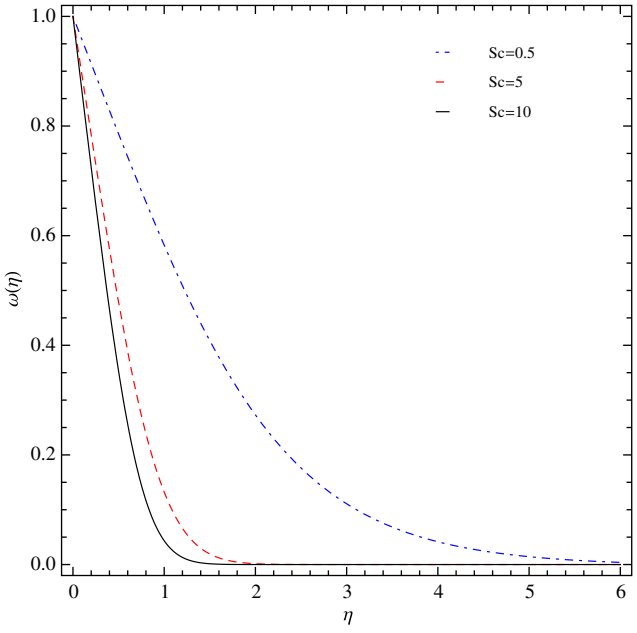

Figure 7 Influence of Sc on $\omega(\eta)$ at $Pr = 0.71$ and $\delta = 0.5$ at the optimal values of $\hbar_1$, $\hbar_2$, and $\hbar_3$.

We now turn to the results which demonstrate the effect of varying the parameter δ. The parameter δ represents the ratio of thermal buoyancy force and the total body force (algebraic sum of gravity, thermal and concentration buoyancy forces). Thus $\delta = 0$ corresponds to zero thermal buoyancy force which means the process is pure mass transfer driven. Similarly, $\delta = 1$ implies a pure heat transfer process. The effect of δ on the velocity distribution in the hydrodynamic boundary is shown in Fig. 8 for $Pr = 0.71$ and $Sc = 0.1$. The highest peak velocity occurs for $\delta = 0$, i.e., for the pure mass transfer process. The lowest peak velocity occurs for $\delta = 1$, i.e., for the pure heat transfer process. The hydrodynamic boundary is thickest for pure mass transfer and thinnest for pure heat transfer with the thickness for simultaneous heat and mass transfer falling in the middle. The pattern exhibited by the present results matches with the results reported in Schenk et al. (1976). The temperature profiles corresponding to the velocity profiles of Fig. 8 are given in Fig. 9. The highest temperatures occur in the pure heat transfer case ($\delta = 1$). The lowest temperature are predicted for the pure mass transfer

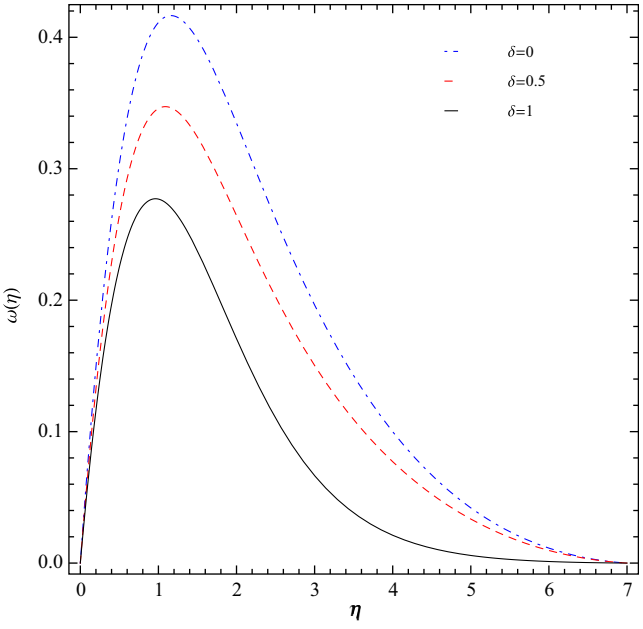

Figure 8 Influence of δ on $f'(\eta)$ at $Pr = 0.71$ and $Sc = 0.1$ at the optimal values of $\hbar_1$, $\hbar_2$, and $\hbar_3$.

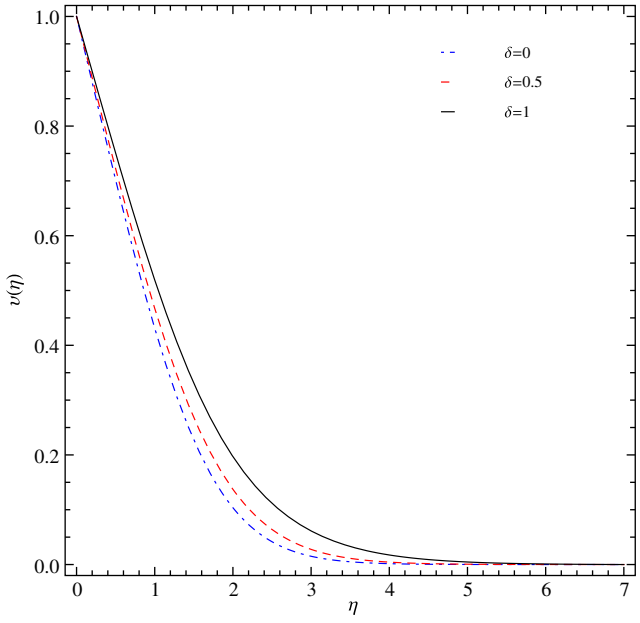

Figure 9 Influence of δ on $\upsilon(\eta)$ at $Pr = 0.71$ and $Sc = 0.1$ at the optimal values of $\hbar_1$, $\hbar_2$, and $\hbar_3$.

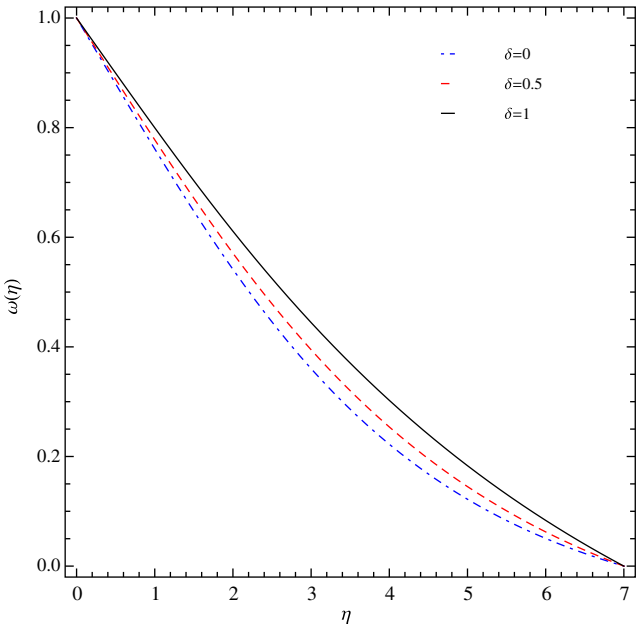

Figure 10 Influence of δ on $\omega(\eta)$ at $Pr = 0.71$ and $Sc = 0.1$ at the optimal values of $\hbar_1$, $\hbar_2$, and $\hbar_3$.

situation. The concentration profiles shown in Fig. 10 for the three values of delta show that the species concentration is highest for the pure heat transfer case and lowest for the pure mass transfer case. The concentration curve for the case of simultaneous heat and mass transfer falls in the middle. The temperature and concentration results presented here corroborate with the results cited in Schenk et al. (1976).

Since the focus of this paper is to demonstrate the usefulness and accuracy of the homotopy analysis method, no attempt has been made to discuss the physical interpretations of the results. In any case, the physical interpretations are well documented in the previous research papers on the problem (Bottemanne, 1972a,b, 1976) and well known to the thermal science research community.

5. Conclusions

The homotopy analysis method has been successfully implemented to develop an analytic solution for simultaneous natural convection and mass transfer from an isothermal vertical plate. The effects of Schmidt number and the buoyancy ratio on the velocity, concentration, and temperature profiles in the respective boundary layers are illustrated with graphs. When compared with the other results reported in the literature, the present results are found to be highly accurate and consistent with the other results pertaining to the same problem. The use of concept of averaged residual recently introduced by Liao (2010) greatly improves the rate of the convergence of the analytic solution by allowing the determination of the optimal auxiliary parameter.

Acknowledgement

This work is partly supported by Bakhtar Institute of Higher Education of Iran.

References

Aziz, A., Khani, F., 2009. Analytic solutions for a rotating radial fin of rectangular and various convex parabolic profiles. Commun. Nonlinear Sci. Numer. Simulat.. doi:10.1016/j.cnsns.2009.07.008.

Bottemanne, F.A., 1972a. Experimental results of pure and simultaneous heat and mass transfer by free convection about a vertical cylinder for Pr = 0.71 and Sc = 0.63. Appl. Sci. Res. 25 (1), 372–382.

Bottemanne, F.A., 1972b. Theoretical solution of simultaneous heat and mass transfer by free convection about a vertical flat plate. Appl. Sci. Res. 25 (1), 37–149.

Darvishi, M.T., Khani, F., 2009. A series solution of the foam drainage equation. Comput. Math. Appl. 58, 360–368.

Gebhart, B., Pera, L., 1971. The nature of vertical natural convection flows resulting from the combined buoyancy effects of thermal and mass diffusion. Int. J. Heat Mass Transfer 14, 2025–2050.

Khani, F., Aziz, A., 2010. Thermal analysis of a longitudinal trapezoidal fin with temperature-dependent thermal conductivity and heat transfer coefficient. Commun. Nonlinear Sci. Numer. Simulat. 15 (3), 590–601.

Khani, F., Ahmadzadeh Raji, M., Hamedi-Nezhad, S., 2009a. A series solution of the fin problem with a temperature-dependent 3 thermal conductivity. Commun. Nonlinear Sci. Numer. Simulat. 14, 3007–3017.

Khani, F., Farmany, A., Ahmadzadeh Raji, M., Aziz, A., Samadi, F., 2009b. Analytical solution for heat transfer of a third grade viscoelastic fluid in non-Darcy porous media with thermophysical effects. Commun. Nonlinear Sci. Numer. Simulat. 14 (11), 3867–3878.

Khani, F., Ahmadzadeh Raji, M., Hamedi Nejad, H., 2009c. Analytical solutions and efficiency of the nonlinear fin problem with temperature-dependent thermal conductivity and heat transfer coefficient. Commun. Nonlinear Sci. Numer. Simulat. 14, 3327–3338.

Liao, S.J., 1999. An explicit, totally analytic approximate solution for Blasius-viscous flow problems. Int. J. Nonlinear Mech. 34 (4), 759–778.

Liao, S.J., 2003. Beyond Perturbation: Introduction to the Homotopy Analysis Method. Chapman & Hall/CRC Press, Boca Raton.

Liao, S.J., 2005. A new branch of solutions of boundary-layer flows over an impermeable stretched plate. Int. J. Heat Mass Transfer 48, 2529–2539.

Liao, S.J., 2009. Notes on the homotopy analysis method: some definitions and theorems. Commun. Nonlinear Sci. Numer. Simulat. 14 (4), 983–997.

Liao, S.J., 2010. An optimal homotopy-analysis approach for strongly nonlinear differential equations. Commun. Nonlinear Sci. Numer. Simulat. 15, 2003–2016.

Liao, S.J., Magyari, E., 2006. Exponentially decaying boundary layers as limiting cases of families of algebraically decaying ones. ZAMP 57 (5), 777–792.

Liao, S.J., Tan, Y., 2007. A general approach to obtain series solutions of nonlinear differential equations. Stud. Appl. Math. 119, 297–355.

Molabahrami, A., Khani, F., 2009. The homotopy analysis method to solve the Burgers–Huxley equation. Nonlinear Anal. Real World Appl. 10 (2), 589–600.

Mollendorf, J.C., Gebhart, B. Axisymmetric natural convection flows resulting from combined buoyancy effects of thermal and mass diffusion, in: Proceedings Fifth International Heat Transfer Confererence, Tokyo, vol. 5, 1974, pp. 10–14.

Schenk, J., Altmann, R., de Wit, J.P.A., 1976. Interaction between heat and mass transfer in simultaneous natural convection about an isothermal vertical flat plate. Appl. Sci. Res. 32 (6), 599–606.

Taunton, J.W., Lightfoot, E.N., Stewart, W.E., 1970. Simultaneous free convection heat and mass transfer in laminar boundary layers. Chem. Eng. Sci. 25 (12), 1927–1937.